



LAWRENCE  
LIVERMORE  
NATIONAL  
LABORATORY

# Migration of positively charged defects in (alpha)-quartz

T. Laino, D. Donadio, I-F. W. Kuo

February 12, 2007

Physical Review B

## **Disclaimer**

---

This document was prepared as an account of work sponsored by an agency of the United States government. Neither the United States government nor Lawrence Livermore National Security, LLC, nor any of their employees makes any warranty, expressed or implied, or assumes any legal liability or responsibility for the accuracy, completeness, or usefulness of any information, apparatus, product, or process disclosed, or represents that its use would not infringe privately owned rights. Reference herein to any specific commercial product, process, or service by trade name, trademark, manufacturer, or otherwise does not necessarily constitute or imply its endorsement, recommendation, or favoring by the United States government or Lawrence Livermore National Security, LLC. The views and opinions of authors expressed herein do not necessarily state or reflect those of the United States government or Lawrence Livermore National Security, LLC, and shall not be used for advertising or product endorsement purposes.

# Migration of positively charged defects in $\alpha$ -quartz

Teodoro Laino,<sup>1,\*</sup> Davide Donadio,<sup>2</sup> and I-Feng W. Kuo<sup>3</sup>

*<sup>1</sup>Physikalisch Chemisches Institut, Universität Zürich,  
Winterthurerstrasse 190, CH-8057 Zürich*

*<sup>2</sup>Computational Science, DCHAB, ETH Zurich, USI Campus,  
Via Giuseppe Buffi 13, CH-6900 Lugano, Switzerland*

*<sup>3</sup>Computational Chemical Biology, Chemistry and Materials Science L-091,  
Lawrence Livermore National Laboratory, Livermore, CA 94550, USA.*

(Dated: March 2, 2007)

## Abstract

We apply a newly developed quantum–mechanics/ molecular–mechanics (QM/MM) scheme to simulate the migration of charged oxygen defects in  $\alpha$ -quartz. We simulate the transition mechanism and compute the potential energy and free energy surface for the puckering of the symmetric charged oxygen vacancy and the formation of the  $E'_1$  center. By overcoming low energy barriers this puckering mechanism can be reiterated allowing the drift of the positive charge localized on an over-coordinated oxygen atom. This process enhances the stability of the  $E'_1$  center and can be regarded as an important channel of structural reorganization of oxygen deficient silica in the presence of strong polarizing electric fields.

KEYWORDS: Silica, QM/MM, Oxygen Vacancy, DFT, NEB.

## I. INTRODUCTION

Silicon dioxide is a material of prime importance in microelectronics and fiber optics. Many of the peculiar properties that make silica such an interesting and versatile material are determined by the presence of defects and impurities. Defects strongly affect the performances of silica as a dielectric in transistors, being responsible for current leakage, but they are also held responsible for some phenomena that are positively exploited in optical fibers, such as photosensitivity, which stands behind the writing of photoinduced Bragg gratings<sup>1</sup> and the generation of second-order non-linear response<sup>2</sup> achieved by poling. The underlying microscopic mechanisms of both these phenomena are still mainly unknown, but they are related to structural rearrangements of the SiO<sub>2</sub> network in correspondence of defects. Among the defects that have a remarkable effect on photosensitivity and poling in silica, it was recently pointed out the role of oxygen deficient centers<sup>3</sup>. Neutral oxygen vacancies in silicon dioxide consist of a covalent bond between two silicon atoms. Upon ionization, the Si-Si bond is weakened and the remaining unpaired electron is delocalized between the two silicon atoms [SiSi<sup>+</sup>]. This configuration is commonly associated with the ESR signal of the E'<sub>5</sub> which is observed in amorphous silica<sup>4,5</sup>. On the other hand no experimental evidence of this defect has been found in  $\alpha$ -quartz so far, which suggests that it is not thermodynamically stable in the crystalline environment as argued in Ref.<sup>6</sup>. In fact, the positively charged oxygen vacancy (OV<sup>+</sup>) can undergo an asymmetric relaxation that localizes the unpaired electron on a three-fold coordinated silicon atom and the hole on the other one. The positively charged silicon atom reverts back and forms an elongated electrostatic bond with a bridging oxygen of the surrounding network, turning into a puckered configuration. This configuration ([Si(3)+O(3)<sup>+</sup>]) consists of a silicon dangling bond and an over-coordinated oxygen atom and is unanimously related to the ESR signal of the E'<sub>1</sub> center<sup>7-13</sup>. The correspondent structure in amorphous silica is dubbed E' <sub>$\gamma$</sub>  center.

Given that it is one of the most abundant point defects in silica and its importance in the degradation of the performances of the gate oxide in transistors, the charged oxygen vacancy has been the subject of a large number of calculations<sup>5,6,14,14-23</sup>. In particular, recent studies<sup>6,15</sup> showed that the positive vacancy is stable only for Fermi levels that lie nearly 3.3 eV above the valence top band of  $\alpha$ -quartz. Hence the positive oxygen vacancy in the configuration [Si(3)+O(3)<sup>+</sup>] can be efficiently created by irradiation followed by a thermal

relaxation or with hole injection techniques. Computationally a partial disagreement is found in literature for the relative energies of the two defect configurations. Blöchl<sup>15</sup> shows that the [SiSi<sup>+</sup>] and the [Si(3)+O(3)<sup>+</sup>] defects are nearly iso-energetic, with the [Si(3)+O(3)<sup>+</sup>] more stable by 0.04 eV, while Boero et al.<sup>14</sup> predicted [Si(3)+O(3)<sup>+</sup>] to be more stable by 0.3 eV. This partial disagreement has been justified with the use of different exchange-correlation functionals in the DFT calculations, in particular Boero et al.<sup>14</sup> used a local density approximation (LDA)<sup>24</sup> as opposed to Blöchl using a gradient-corrected functional<sup>25</sup>. The Barrier of the conversion  $E'_\delta - E'_1$  has been calculated<sup>15</sup> to be 0.38 eV, in agreement with Boero et al.<sup>14</sup>. Other quantum chemical studies<sup>5</sup> predict [Si(3)+O(3)<sup>+</sup>] to be more stable by 0.64 eV with a barrier between the two defects of 0.38 eV. Unfortunately the structures of these cluster calculations differ sizably from the DFT based calculations<sup>14,15</sup> possibly due to the use of Hartree-Fock for computing optimized geometries. As this defect is known to generate an important strain field in the silica matrix<sup>26-28</sup> we argue that the way the boundary conditions are treated can be another very important source of discrepancies in the calculation of the energetics.

From the barrier of 0.38 eV for the transition between [SiSi<sup>+</sup>] and [Si(3)+O(3)<sup>+</sup>], one would expect to see both configurations in about equal concentrations, whereas in isochronal annealing studies, performed on amorphous silica, the  $E'_\gamma$  center apparently anneals at much higher temperature than  $E'_\delta$ <sup>4</sup>. Thus there is still an open issue related to the apparent higher stability of the  $E'_\gamma$  center compared to the  $E'_\delta$ . Blöchl<sup>15</sup> suggested that the concentration measured in isochronal annealing experiments does not only reflect thermal stability, but also a possible charge-transfer process that makes the defect ESR invisible. The arguments used to validate this speculation are mainly based on relative stability of the electronic levels between the oxygen charge and neutral vacancy defects. In fact, the charging level of  $E'_\delta$  lies 1.38 eV below the silicon mid-gap, where it can capture electrons from other filled defect states or the contacts while the charging level of  $E'_\gamma$  lies 0.68 eV above it.

Starting from an ionized OV, using a newly developed QM/MM scheme<sup>29</sup> implemented into the CP2K code<sup>30</sup>, we compute the transition path, the potential energy barrier and the free energy barrier for the puckering and formation of an  $E'_\gamma$  (known as  $E'_1$  in  $\alpha$ -quartz) center and a three-fold coordinated oxygen atom. The QM/MM approach employed here allows for an accurate description of the defect-induced strain field in the crystal, which provides a better estimate of the energetics of the defects configurations with respect to

previous published results<sup>14,15</sup>.

Here we propose an alternative mechanism, based on the migration of the three-fold coordinated oxygen atom through the quartz pattern, that concurs to stabilizing the  $E'_1$  over the  $E'_\delta$ . On the basis of our computational evidences, we propose that once the  $E'_1$  center is formed, it can easily access a large number of states, we will call  $E_1^*$ , ESR similar to the  $E'_1$ , characterized by a migration of the three-fold oxygen defect through the crystal. Moreover we propose for the first time a process of structural rearrangement in silica associated to a directional charge migration, which does not involve the existence of ionic impurities. Since this process is accompanied by the drift of the positive hole, we suggest that the puckering mechanism can be substantially enhanced by the application of an external electric field, resulting in a migration of the positive charge assisted by the migration of the three-fold coordinated oxygen atom. These concepts can be extended to amorphous system except for directionality which is peculiar of the quartz crystal. Although the study of the amorphous system would be technologically more relevant, it would have required a statistical analysis, which is unaffordable for present day computer resources. We have therefore chosen to study defect transformations in  $\alpha$ -quartz which saves us from sampling over a large amount of different sites.

## II. METHODS

We have performed QM/MM geometry optimizations, molecular dynamics and optimization of reaction path to describe quantitatively the energetics along the coordinate linking the  $E'_\delta$ ,  $E'_1$  and  $E_1^*$ . The calculations presented are based on a QM/MM scheme previously tuned and tested on  $\alpha$ -quartz<sup>29,31</sup>. A DFT<sup>32,33</sup> level of theory with local spin density (LSD) approximation to treat the open shell system is used for the description of the quantum region. The exchange-correlation functional employed in the overall calculation is PBE<sup>25,34</sup> and a cutoff of 250 Ry is used for the expansion of the QM electronic density. The classical force-field used to describe the MM system subsystem is the van Beest, Kramer, van Santen (BKS) potential<sup>35</sup> already extensively tested for QM/MM simulations of  $\alpha$ -quartz<sup>29</sup>. The link between the QM and the MM region is performed through the use of modified pseudopotential as already described in<sup>29</sup>. All calculations have been performed with the CP2K package. The wave-function optimization is performed by the Quickstep algorithm<sup>36</sup> using

a dual basis set (BS): a Gaussian BS to construct the Hamiltonian core matrix and a plane wave BS to evaluate the exchange-correlation and Hartree potential.

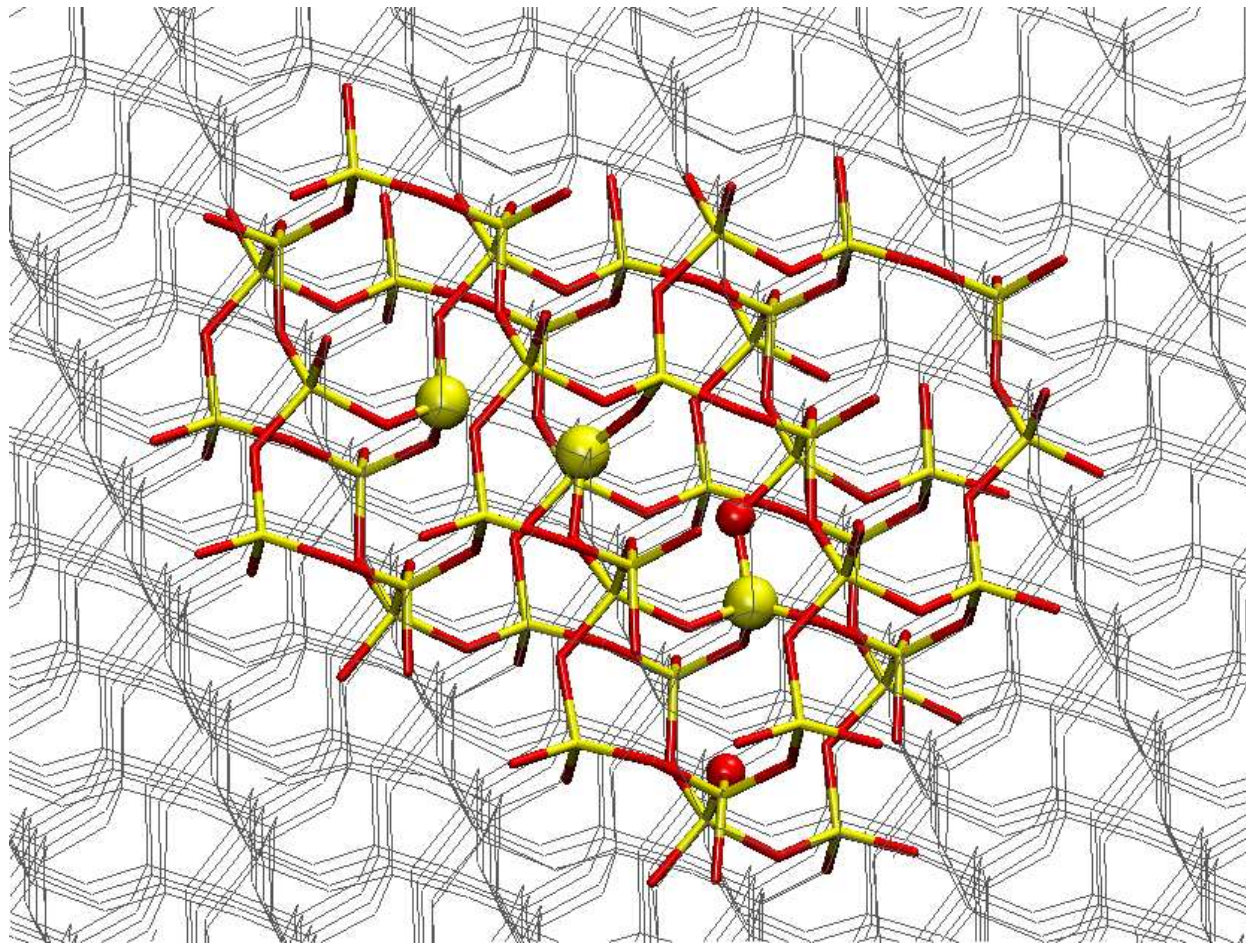


FIG. 1: Structure of the QM fragment embedded in the MM crystal. Atoms involved into the migration of the charged OV are depicted with bigger dots

The MM quartz crystal made of 5184  $\text{SiO}_2$  units (15552 atoms) in an orthorhombic cell with lattice constants of 49.94 Å, 57.66 Å and 63.49 Å is optimized using the BKS pair potential<sup>35</sup> which provides a reliable description of bulk  $\alpha$ -quartz. After removal of an oxygen atom, a portion of 159 atoms was chosen in order to surround the OV defect and to suitably describe the motion of the defect through the crystal Fig.(1). The oxygen boundary atoms is described with a core charge increased by 0.4  $e$  in order to maintain the neutrality of the overall system. This boundary scheme has been extensively tested in a recent publication<sup>29</sup>.

The QM/MM potential is efficiently computed exploiting the Gaussian expansion of the electrostatic potential (GEEP) scheme<sup>37</sup>. The long-range electrostatic term in the QM/MM coupling scheme is essential to treat properly the quantum properties of the QM subsystem in ordered structures (like  $\alpha$ -quartz), unless carefully designed MM cluster are used<sup>31</sup>. The inclusion of the periodic boundary conditions in the evaluation of the SCF perturbing MM external potential is achieved introducing a reciprocal space term of the MM electrostatic potential through a modified Ewald scheme<sup>31</sup>. Moreover the QM subsystem is coupled to its own periodic images using the same scheme recently implemented to decouple periodic images in PW-based QM calculations<sup>38</sup>. QM/MM geometry optimizations have been performed on the three local minima identified with the defects  $E'_\delta$ ,  $E'_1$  and  $E_1^*$  Fig.(2).

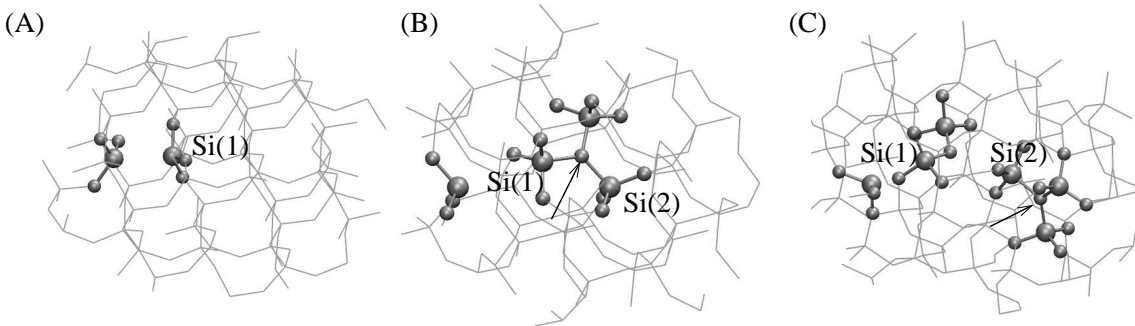


FIG. 2: Locally stable structures of the positively charged oxygen vacancy: the symmetric charged OV ( $E'_\delta$ )(panel A), the puckered configuration ( $E'_1$ ) with the positive charged localized on the three-fold coordinated oxygen (B) and the configuration obtained after the migration of the three-fold coordinated oxygen ( $E_1^*$ )(C). Large spheres represent silicon atoms while smaller ones are oxygen atoms. The arrows indicate the three-fold coordinated oxygens in panels (B) and (C).

Once defined the structure of the three local minima, we have performed a full mapping of the energetics of the reaction path going from  $E'_\delta$  to  $E_1^*$  passing through  $E'_1$ . The reaction path has been computed with a nudged elastic band calculation<sup>39–41</sup> using the module implemented into the CP2K code. The optimization of the band has been performed by a coupled steepest descent/DIIS procedure with a tolerance of 0.001 a.u. on gradients.

To complete the description with a finite temperature reaction path, we have performed meta-dynamics<sup>42</sup> calculations in order to compute the free energy profile as a function of

suitably defined reaction coordinates.

### III. RESULTS AND DISCUSSION

#### A. Equilibrium Geometries

A neutral OV is created by removing an oxygen atom from a QM fragment of the fully optimized MM crystal (15552 atoms), and the corresponding structure has been relaxed at the QM/MM level. A covalent bond is formed between the two silicon atoms separated by 2.34 Å. When an electron is removed from the system this covalent bond is weakened and the distance between the two silicon atoms increases to 2.85 Å. We have verified that this structural conformation Fig.(3-a), identified with the ( $E'_\delta$ ) center, is stable in a MD run of 5.0 ps long at room temperature (398K).

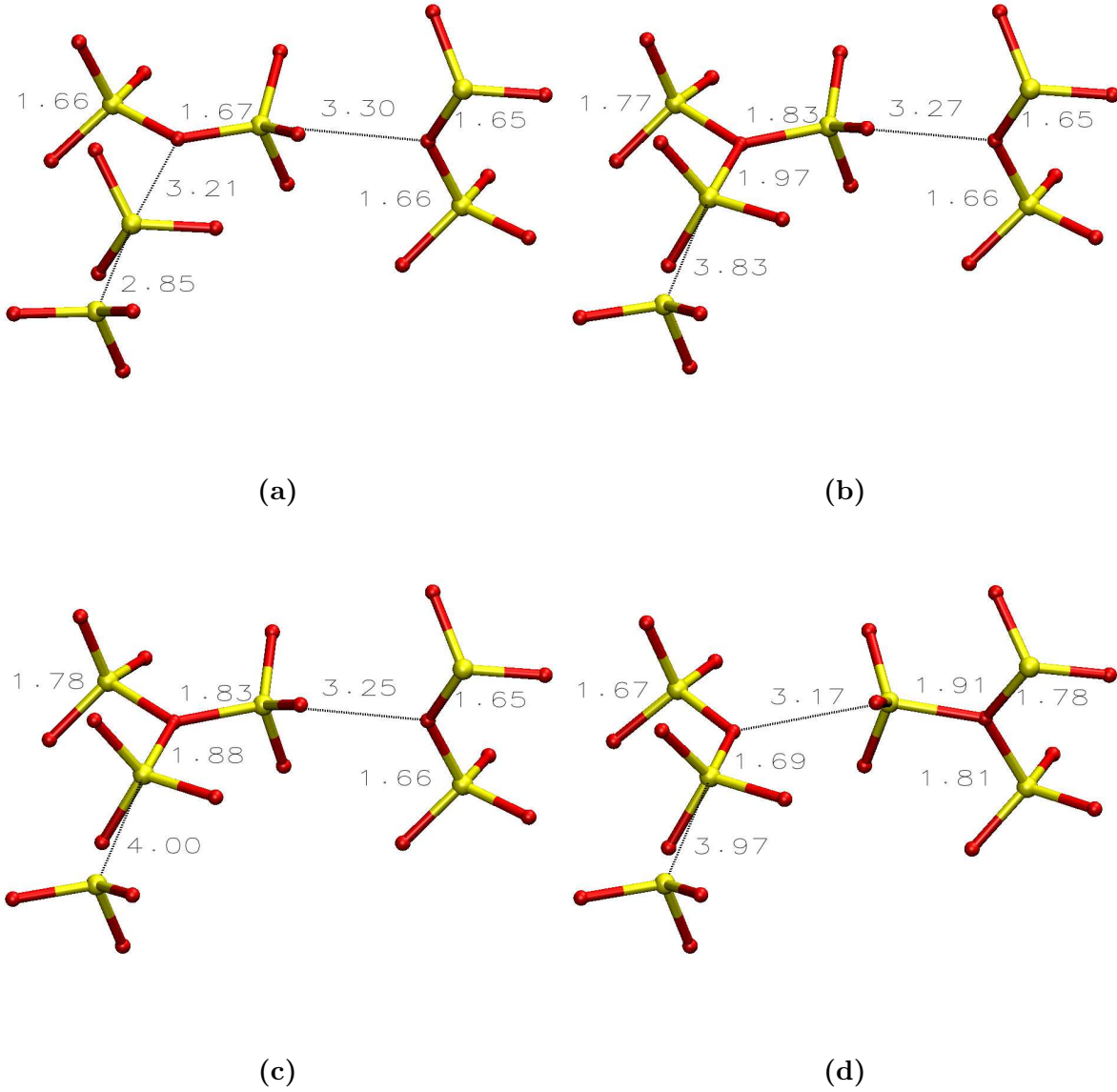
Another locally stable structure is obtained by puckering one of the silicon atoms<sup>14,15</sup> Fig.(3-a) and Fig.(3-b). In qualitative agreement with Ref.<sup>14,15</sup>, we find that this configuration, identified as the  $E'_1$  center, is more stable than the initial  $[\text{SiSi}^+]$  conformation, being the relative total energy difference 0.18 eV. The quantitative disagreement in this stabilization energy with respect to previously published data (0.04 eV<sup>15</sup> and 0.30 eV in<sup>14</sup>) may be due to different reasons. As in Ref.<sup>15</sup> we performed all calculations using a gradient-corrected exchange-functional, while Boero et al.<sup>14</sup> were using plain LDA. Another source of difference may be represented by the open-shell DFT treatment, however in previous works it was shown that geometries and energies of the  $E'_\gamma$  center in amorphous silica do not change switching from LDA to LSD<sup>43</sup>. The largest source of discrepancy between our work and the previous ones is certainly that the QM/MM scheme allows large systems to be simulated, thus providing a more realistic treatment of the defect induced strain field, which can extend for up to five coordination shells in the case of oxygen deficiency centers<sup>26,27</sup>. In addition, the system size used in Ref.<sup>14</sup> and Ref.<sup>15</sup> is also too small to avoid a strong interaction between the charged periodic replica, while in our case the QM charged system interact with a periodicity that is the one of the full MM crystal ( $\approx 60$  Å against  $\approx 10$  Å) and the periodic interaction is screened by the presence of the MM charge distribution.

Interestingly, while performing geometry optimization of the puckered configuration we found two iso-energetic local minima (see Fig.(3-b) and Fig.(3-c)), differing slightly in the

coordination distances of the three-fold oxygen atom. In particular the distance of this oxygen from the puckered Silicon can change of 0.1 Å from one minima to the other. In this latter configuration two of the three distances Si-O around the three-folded oxygen atom are almost equivalent, while the third is constantly 0.1 Å smaller. The equivalence between these two bonds suggest that the puckering mechanism can be iterated by breaking a pre-existing Si-O bond around the over-coordinated oxygen. The resulting silicon atom can revert back and binds to another bridging oxygen which becomes 3-fold coordinated Fig.(3-d), what we call in this paper  $E_1^*$ . This transformation is also accompanied by the migration of the positive charge that moves farther apart from the paramagnetic silicon center as it gets localized on the newly formed 3-fold coordinated oxygen atom.

Also for this structure, here labeled  $E_1^*$ , we highlight the presence of two longest bonds around the new three-fold oxygen atom involving the recently puckered Silicon and the Silicon atom having the right geometrical characteristic to perform a new puckering motion. The  $E_1^*$  Fig.(3-d) is less stable than the original  $E_1'$  by 0.41 eV, but as the process can be iterated until another point defect is found, there is a large number of such configurations available, which are indistinguishable from the pristine  $E_1'$  defect<sup>46</sup>. This makes the ensemble of these metastable states relevant to the kinetics and thermodynamics of defects in  $\alpha$ -quartz and possibly in amorphous silica, in spite of the higher formation energy. For example if we have a concentration of  $E_1'$  centers of  $10^{15}/\text{cm}^3$ , there are  $\sim 10^6$  available migration sites, with a relative chance of being populated with respect to the  $E_1'$  equal to  $P(E_1^*)/P(E_1') = e^{-\Delta E/kT}$  each. Given the energetics reported above, at room temperature this ratio is  $10^{-3}$ , which multiplied by the number of available  $E_1^*$  sites, gives a relative population of the  $E_1^*$   $10^3$  times larger than the  $E_1'$  and similar to the  $E_1'$ . Increasing the temperature or reducing the defect concentration moves this balance even more on the side of the  $E_1^*$ . The migration path is predetermined to be helical on the basis of quartz chirality, since only 2 out of the 3 silicon atoms coordinating the oxygen atom have a neighboring oxygen atom at  $\approx 3.0$  Å on which the puckering leads to a metastable structure.

FIG. 3: These frames show the relevant bond distances for the several optimized geometry structures at QM/MM level. For clarity reason only atoms involved in the migration of the OV defects are shown. Frame Fig.(3-a) shows the  $E'_8$ , obtained relaxing the OV after charging the defect. Frame Fig.(3-b) and Fig.(3-c) show two local iso-energetic minima of the  $E'_1$  defect. the two structures differ of few picometers in the bond distances around the three-fold oxygen atoms. The last frame Fig.(3-d) shows the migrated defect, called in this work  $E_1^*$ .



## B. Migration path energy profile

Using the above mentioned optimized structures we have performed a nudged elastic band (NEB)<sup>39–41</sup> optimization of the transition path to describe the energetics of the migration of the defect from  $E'_\delta$  to  $E_1^*$  through  $E'_1$ . The calculation has been performed using the NEB module as implemented in CP2K, interpolating 16 more images between the 4 optimized geometries, in order to have all images roughly at the same distance. A spring constant of 0.03 a.u. was used to describe the spring force between replicas together with the IT-NEB<sup>41</sup> algorithm to avoid the formation of kinks. A coupled steepest descent/DIIS optimization has been used to optimize the band. The 20 replicas used to describe the full migration path were computed using 64 processors per replica (1280 processors in total) and the optimization procedure required 188 optimization steps to achieve the convergence criteria on gradients (0.001 a.u.). The full band optimization required 200K cpu hours to be completed<sup>44</sup>. The optimized energy profile is shown in Fig.(4) and it clearly shows that defects  $E'_\delta$  and  $E'_1$  are separated by a barrier of 0.14 eV, value smaller than the one reported by<sup>14,15</sup> of 0.38 eV. Same considerations done for the optimized energies holds for the quantitative disagreement between this work and the previous ones<sup>14,15</sup> regarding transition state energies. Moreover defects  $E'_1$  and  $E_1^*$  are separated by a barrier of 0.59 eV, that can be relatively easily overcome even at room temperature. The barriers between  $E_1^*$  states are expected to be even lower, so that the puckering mechanism can continue along the crystal pattern.

## C. Charge analysis and energy levels

The charged oxygen deficient centers studied in this paper are all open-shell systems. In order to validate the results obtained we checked that the self-interaction error<sup>24,45</sup> in this system was not a vitiating source of error. Indeed the analysis of the spin-density shows that it is very localized around the under-coordinate silicon atom. This confined spin-density reflects in a negligible error due to the interaction of the electron with itself.

It's interesting to note that the migration of the three-fold coordinated oxygen is tightly couple to the migration of the positive charge. The population analysis is a by-product of the coupling/decoupling scheme. In fact the charged used to restore the proper peri-

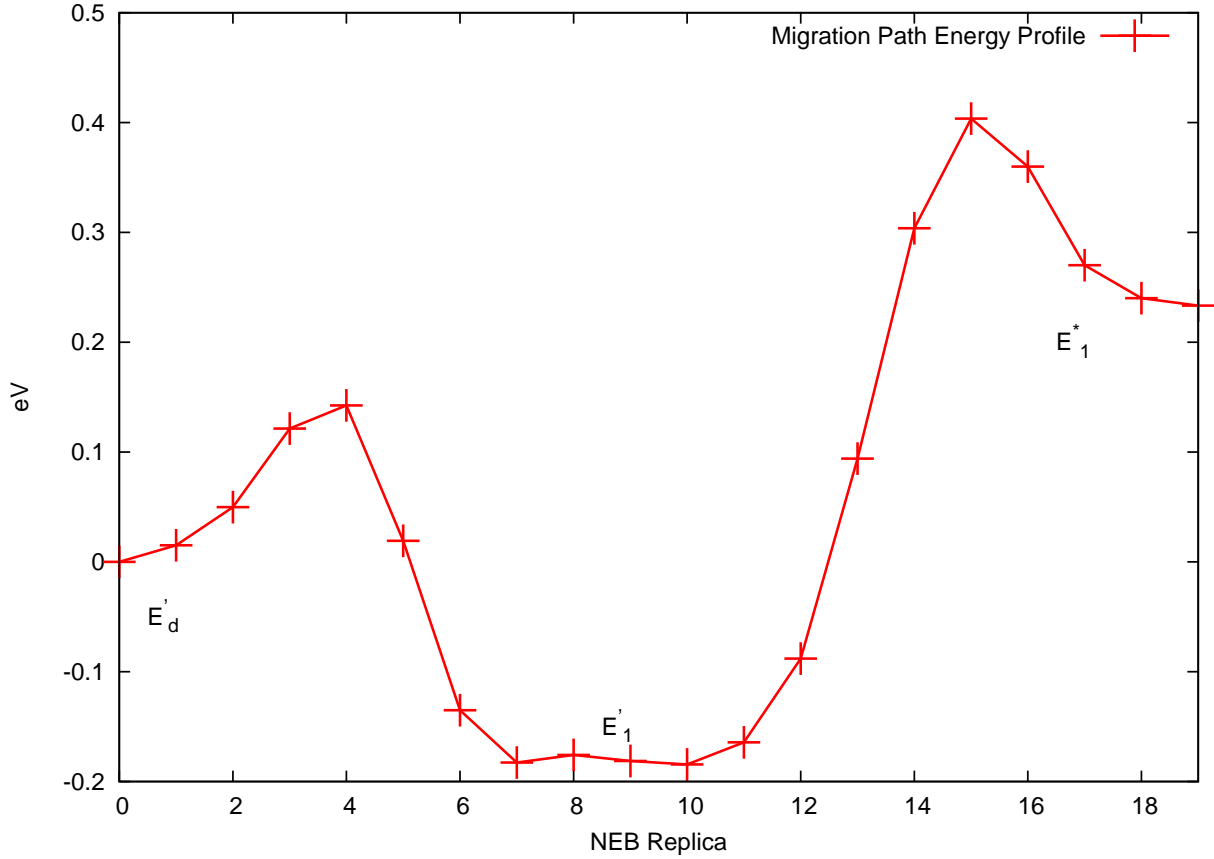


FIG. 4: Optimized energy path from  $E'_\delta$  to  $E_1^*$  through  $E'_1$ .

odicity for the QM system<sup>31,38</sup> reproduce correctly the amount of charge present on each atom<sup>38</sup>. A Löwdin population analysis was performed for comparison and results for both methodologies were in good agreement. In the defect  $E'_\delta$  the positive charge is delocalized between the two silicon atoms. After the first puckering the positive charge is mainly localized over the three-fold oxygen atom (+0.49 e) with a small delocalization over the Silicon atoms surrounding the oxygen (+0.17 e), while the unpaired electron is located on the under-coordinated silicon atom. The same behavior is observed for the defect  $E_1^*$ , the positive charge being totally localized around the three folded oxygen atom, with a main localization over the oxygen itself (+0.64 e). An interesting aspect is also provided by the energy level of the unpaired electron.

In Fig.(5) we have shown the density of states (DOS) for the three configurations, providing different DOS for  $\alpha$  and  $\beta$  spin. The DOS was obtained averaging the states levels during 5

ps of MD simulation at 398K (all configurations were stable during a microcanonical MD at 398K for the simulated time of 5 ps). It is unmistakable from this picture that the energy level of the defect rises going from C1 to C2 and then C3 (see Fig.(5-a), Fig.(5-c) and Fig.(5-e)). In Fig.(6) we show the energy level of the defect along the optimized migration path, the zero being the energy level of an electron in highest level the Kohn-Sham valence band. As we can see the energy level increases along the migration  $E'_\delta \rightarrow E_1^*$ . The energy level of  $E_1^*$  is higher of 1.95 eV with respect to  $E'_\delta$  and roughly equivalent (0.1 eV smaller) than  $E_1^*$ . Both qualitative and quantitative picture of the energy levels totally agree with previously reported calculations<sup>15</sup>.

#### D. Free Energy calculation

In order to compute the free energy barrier we have applied the metadynamics method selecting the out of plane angles of the two puckering silicon atoms as collective variable. We have used hills with height of  $10^{-3}$ , Hartree and width of 0.05 a.u., spawned each 20 fs of MD simulation. The free energy profile is shown in figure Fig.(7). In the free energy framework the energy difference between the  $E_1^*$  and the  $E'_\delta$  defects, is much smaller (0.04 eV) than the value determined with the band calculation, while the barrier is higher (0.33 eV) with respect to the value found in the 0K NEB. Regarding the transformation from  $E_1^* \rightarrow E'_\delta$  we found in the free energy the same value for the barrier (0.63 eV) as the one found with the NEB calculation while the difference in the stabilization energy of the two defects is smaller, being 0.33 eV. Apart from slight numerical disagreement the picture of the free energy calculation confirms qualitatively the possibility of the proposed mechanism.

## IV. CONCLUSIONS

In this paper we study the migration path of oxygen charged defects in  $\alpha$ -quartz. On the basis of transition state energies and equilibrium stability we conjecture that the well known process going from defect  $E'_\delta$  to  $E_1^*$  can take place in an iterative way along the crystal path

leading to a charge migration far from the OV site, providing an alternative explanation to available controversial experimental data<sup>4</sup>. In fact, the low free energy barriers computed for both processes ( $<0.6\text{eV}$ ) suggest that the positive charge can easily migrate during the thermal annealing and several equivalent states can be populated providing the same  $E'_1$  ESR signal. After annealing only configurations where the paramagnetic center and the 3-fold coordinated oxygen are close to one another can easily recombine to the energetically more favored  $E'_g$  structure, while if the positive charge migrates farther apart recombination will be unlikely to happen. Therefore our result provides a convincing explanation for the apparent higher stability of the  $E'_1$  center. In the presence of an external electric field, as in the case of poling, this mechanism would be enhanced, providing a viable path to a permanent structural modification associated to the drift of positive charges.

---

\* `tlaino@pci.uzh.ch`

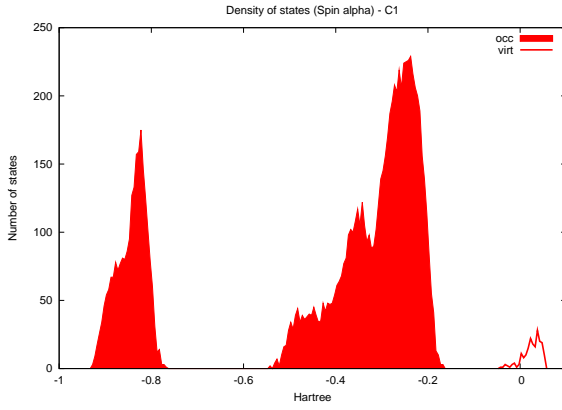
- <sup>1</sup> K. O. Hill, Y. Fujii, D. C. Johnson, and B. S. Kawasaki, *Appl. Phys. Lett.* **32**, 647 (1978).
- <sup>2</sup> R. A. Myers, N. Mukherjee, and S. Brueck, *Opt. Lett.* **16**, 1732 (1991).
- <sup>3</sup> E. Franchina, C. Corbari, P. Kazansky, N. Chiodini, A. Lauria, and A. Paleari, *Solid State Comm.* **136**, 300 (2005).
- <sup>4</sup> D. Griscom and E. J. Friebele, *Phys. Rev. B* **34**, 7524 (1986).
- <sup>5</sup> G. Pacchioni and G. Ierano, *Phys. Rev. Lett.* **81**, 377 (1998).
- <sup>6</sup> C. Carbonaro, V. Fiorentini, and F. Bernardini, *Phys. Rev. Lett.* **86**, 3064 (2000).
- <sup>7</sup> C. M. Nelson and R. A. Weeks, *J. Am. Ceram. Soc.* **43**, 396 (1960).
- <sup>8</sup> R. A. Weeks, *J. Appl. Phys.* **27**, 1376 (1956).
- <sup>9</sup> R. A. Weeks and C. M. Nelson, *J. Am. Ceram. Soc.* **43**, 399 (1960).
- <sup>10</sup> R. H. Silsbee, *J. Appl. Phys.* **32**, 1459 (1961).
- <sup>11</sup> M. G. Jani, R. B. Bossoli, and L. E. Halliburton, *Phys. Rev. B* **27**, 2285 (1983).
- <sup>12</sup> W. L. Warren, E. H. Poindexter, M. Offenbergl, and W. Müller-Warmuth, *J. Electrochem. Soc.* **139**, 872 (1992).
- <sup>13</sup> E. H. Poindexter and W. L. Warren, *J. Electrochem. Soc.* **142**, 2508 (1995).
- <sup>14</sup> M. Boero, A. Pasquarello, J. Sarnthein, and R. Car, *Phys. Rev. Lett.* **78**, 887 (1997).
- <sup>15</sup> P. E. Blöchl, *Phys. Rev. B* **62**, 6158 (2000).

- <sup>16</sup> K. C. Snyder and W. B. Fowler, Phys. Rev. B **48**, 13238 (1993).
- <sup>17</sup> D. C. Allan and M. P. Teter, J. Am. Ceram. Soc. **73**, 3247 (1990).
- <sup>18</sup> F. J. Feigl, W. L. Fowler, and K. L. Yip, Solid State Comm. **14**, 225 (1974).
- <sup>19</sup> K. L. Yip and W. B. Fowler, Phys. Rev. B **11**, 2327 (1975).
- <sup>20</sup> E. P. O'Reilly and J. Robertson, Phys. Rev. B **27**, 3780 (1983).
- <sup>21</sup> A. H. Edwards and W. B. Fowler, J. Phys. Chem. Solids **46**, 841 (1985).
- <sup>22</sup> J. K. Rudra and W. B. Fowler, Phys. Rev. B **35**, 8223 (1987).
- <sup>23</sup> G. Pacchioni, A. M. Ferrari, and G. Ierano, Faraday Discuss. **106**, 155 (1997).
- <sup>24</sup> J. Perdew and A. Zunger, Phys. Rev. B **23**, 5048 (1981).
- <sup>25</sup> J. P. Perdew, K. Burke, and M. Ernzerhof, Phys. Rev. Lett. **77**, 3865 (1996).
- <sup>26</sup> A. Mysovsky, P. Sushko, A. E. S. Mukhopadhyay, and A. Shluger, Phys. Rev. B **69**, No.085202 (2004).
- <sup>27</sup> V. Sulimov, P. Sushko, A. S. A.H. Edwards, and A. Stoneham, Phys. Rev. B **66**, 24108 (2002).
- <sup>28</sup> V. B. Sulimov, V. O. Sokolov, E. M. Dianov, and B. Poumellec, QUANTUM ELECTRON **26**, 988 (1996).
- <sup>29</sup> F. Zipoli, T. Laino, A. Laio, M. Bernasconi, and M. Parrinello, J. Chem. Phys. **124**, No. 154707 (2006).
- <sup>30</sup> The CP2K developers group (2007), freely available at the URL:: <http://cp2k.berlios.de>, released under GPL license.
- <sup>31</sup> T. Laino, F. Mohamed, A. Laio, and M. Parrinello, J. Chem. Theory Comp. **2**, 1370 (2006).
- <sup>32</sup> P. Hohenberg and W. Kohn, Phys. Rev. B **136**, B864 (1964).
- <sup>33</sup> W. Kohn and L. J. Sham, Phys. Rev. **140**, A1133 (1965).
- <sup>34</sup> J. Perdew and Y. Wang, Phys. Rev. B **45**, 13244 (1992).
- <sup>35</sup> B. W. H. van Beest, G. J. Kramer, and R. A. van Santen, Phys. Rev. Lett. **64**, 1955 (1990).
- <sup>36</sup> J. VandeVondele, M. Krack, F. Mohamed, M. Parrinello, T. Chassaing, and J. Hutter, Comp. Phys. Comm. **167**, 103 (2005).
- <sup>37</sup> T. Laino, F. Mohamed, A. Laio, and M. Parrinello, J. Chem. Theory Comp. **1**, 1176 (2005).
- <sup>38</sup> P. E. Blöchl, J. Chem. Phys. **103**, 7422 (1995).
- <sup>39</sup> G. Mills and H. Jónsson, Phys. Rev. Lett. **72**, 1124 (1994).
- <sup>40</sup> G. Mills, H. Jónsson, and G. Schenter, Surf. Sci. **324**, 305 (1995).
- <sup>41</sup> G. Henkelman and H. Jónsson, J. Chem. Phys. **113**, 9978 (2000).

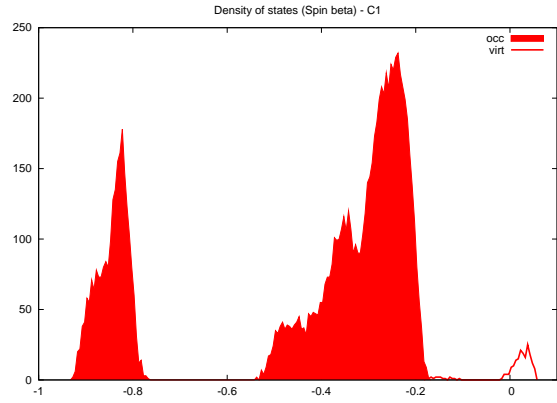
- <sup>42</sup> A. Laio and M. Parrinello, *Procs. Nat. Acad. Sci.* **99**, 12562 (2002).
- <sup>43</sup> D. Donadio, M. Bernasconi, and M. Boero, *Phys. Rev. Lett.* **87**, 195504 (2001).
- <sup>44</sup> Part of this work was performed under the auspices of the U.S. Department of Energy by the University of California Lawrence Livermore National Laboratory under contract No. W-7405-Eng-48.
- <sup>45</sup> Y. Zhang and W. Yang, *J. Chem. Phys.* **109**, 2604 (1998).
- <sup>46</sup> We argue that the  $E_1^*$  structure cannot be distinguished from the  $E_1'$  by ESR, as the influence a positive charge at more than 4-5 Å on the spin localization on the three fold coordinated silicon atom is negligible.

This work performed under the auspices of the U.S. Department of Energy by Lawrence Livermore National Laboratory under Contract DE-AC52-07NA27344.

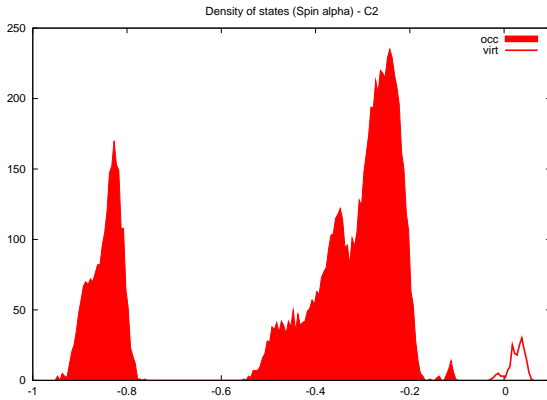
FIG. 5: These frames show the density of states, divided between spin  $\alpha$  and  $\beta$ , of the three configurations:  $E'_\delta$ ,  $E'_1$  and  $E_1^*$ . In particular the comparison between frames Fig.(5-a), Fig.(5-c) and Fig.(5-e), shows that the energy level of the defect increases in energy going from  $E'_\delta$  to  $E'_1$  and  $E_1^*$ . The Energy level of the defect is not identifiable for  $E'_\delta$  (see Fig.(5-a) and Fig.(5-b)) while for  $E'_1$  and  $E_1^*$  it can easily identified at 0.09-0.1 Hartree from the top valence band (see Fig.(5-c) and Fig.(5-e)). For completeness also the density of states of the spin  $\beta$  have been provided.



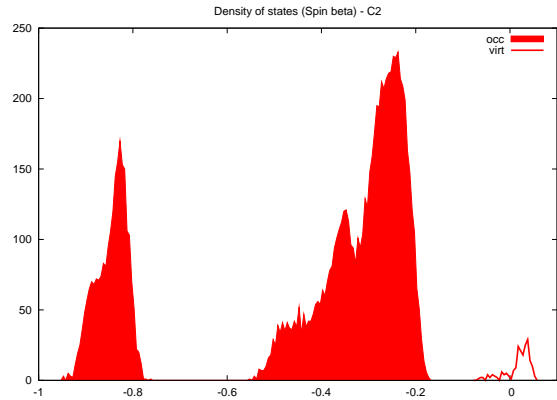
(a)



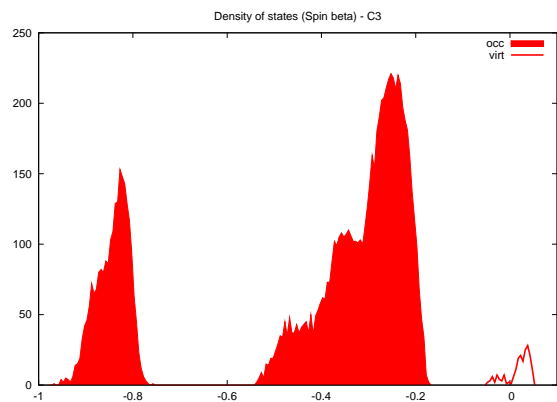
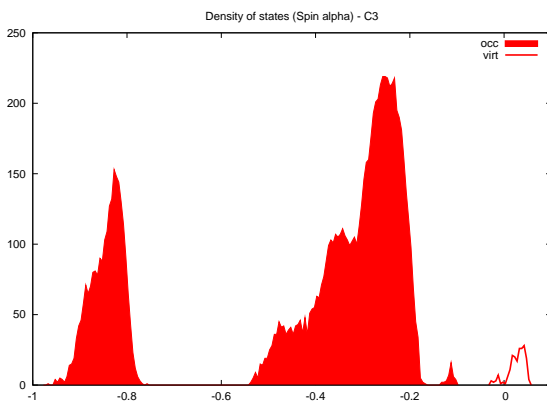
(b)



(c)



(d)



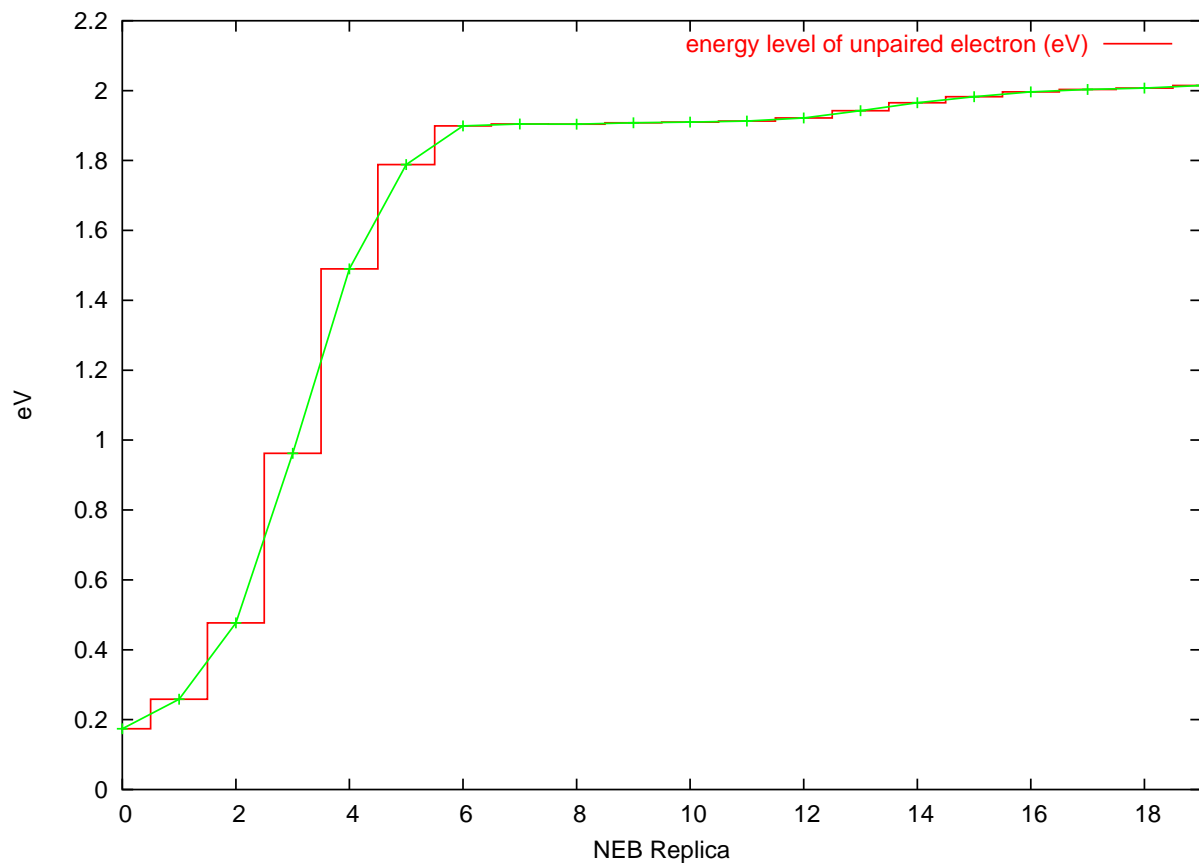


FIG. 6: This picture shows the energy levels of the unpaired electron along the optimized path from  $E'_5$  to  $E_1^*$  through  $E'_1$ .

FIG. 7: On the right the free energy profile for the transition  $E'_\delta \rightarrow E'_1$  while for the process  $E'_1 \rightarrow E_1^*$ .

